Model Predictive Control of Grid Connected Solar PV Inverter

Cameron Smith, *Student Member, IEEE,* Ameen Gargoom, *Senior Member, IEEE,* M. E. Haque, *Senior Member, IEEE,* and Aman Oo, *Senior Member, IEEE*

***Abstract*—The large-scale integration of Solar photovoltaic (PV) systems in the distribution grid has introduced several technical challenges such as voltage variations, reverse power flow, power quality and harmonics. These issues are more pronounced in weak grids. Therefore, modern power inverters with the capacity to complete Volt-Var control and moderate power outputs are required to increase grid stability in weak and/or microgrid installations.**

This paper investigates the use of a Continuous Control Set Model Predictive Control (CCS-MPC) algorithm to control a solar PV inverter, moderating active, and reactive power transfer into the grid through an iterative process. A MATLAB Simulink model is produced and tested to validate the proposed algorithm, with a scenario showing reactive power compensation through Volt-Var control curves. The simulation results confirm that the MPC controller can regulate power flow into the grid with enhanced dynamic and steady state performance, and improved power quality.

***Index Terms*—CCS-MPC, PV, inverter, grid-connect, reactive power control, Volt-Var**

I. Introduction

THE increasing penetration of distributed generation has posed some technical challenges to grid operators, as the use of Grid-Following (GFL) type inverters degrades local power quality in some feeders [1]. These type of inverters are unable to moderate local reactive power levels through injecting or absorbing reactive power as required, and this control is vital to improving local power quality in an AC grid [2]. Standards for Inverter Energy Systems (IES) are changing to consider new demands for active and reactive power control, such as a Frequency-Watt and/or Volt-Var response curves [3] [4]. These changes allow for a Grid-Forming (GFM) type inverter to be implemented, and thus, increasing power quality in local areas [5] [6]. Such inverters can act as a voltage or current source and actively compensate for poor local grid conditions.

IEEE 1547-2018 proposes new requirements for advanced inverters, including the voltage-reactive power mode (Volt-Var) [4]. Load variations and disturbances in a local area can cause voltage fluctuations, and with inverters being able to sink or inject reactive power, voltage regulation without classical compensation is possible.

Current PV inverter control utilises cascaded linear control, through a series of nested feedback loops under PI control [7]. Constantly varying DC bus voltage through PV output fluctuations can cause a degradation of the AC output voltage, with the transient dynamics of cascaded linear control can lead to oscillations [8]. In addition, in areas of high renewable penetration, power control and sharing algorithms will neglect the internal system dynamics, leading to poor control due to interactions of control loops of paralleled inverters [9]. PI control can be difficult to tune due to controller bandwidth and grid coupling, with [10] proposing a linear quadratic method for gains tuning.

Model Predictive Control (MPC) is an accelerating area of research, with advantages over the typical PI control methodology being evident in non-linear systems [11]. By modelling the system to be controlled in discrete time, the control will be able to predict the next output state requirement and modify the system dynamics to suit.

An advantage of MPC over PI control is the ability to assign weightings to a particular desired outcome such as reactive power control, output frequency compensation, switching frequency, battery storage and DC link capacitor voltage balancing [12] [13] [14].

These weighting factors currently rely on a heuristic approach, with research into Artificial Neural Network methods presented in [15]. A novel method presented in [16] focuses on an auto-tuning method for weighting factor selection, and [17] uses an iterative approach for every MPC cycle, selecting a weighting factor of zero initially.

The main features of MPC include the following:

- Fast response to varying grid conditions
- Accurate in non-linear transient conditions
- Control of multiple variables in coupled systems
- Relatively straight-forward design procedure
- Use of finite-time horizon to optimise future outputs as well as the current

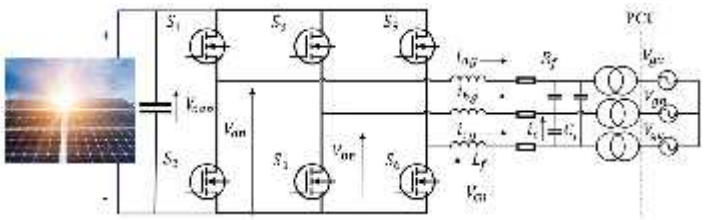

Fig. 1. High-level overview of MPC inverter model

This paper covers the design methodology of a MPC grid-tie inverter with Volt-Var control, and validates the design using MATLAB SimPowerSystem. A scenario with changing loads and local voltage levels is used to demonstrate reactive power compensation and its effects on grid voltage.

This paper will detail the design and modelling of a grid-tie PV inverter and filter, and demonstrate the iterative MPC algorithm. A scenario is presented with reducing the local grid voltage with a heavy load, and measuring the compensation of the inverter through a reactive power injection.

The paper is organized as follows. An overview of the inverter model and control is presented in Section II. The setup and scenario for MATLAB SimPowerSystems is detailed in Section III, with the results shown in Section IV. Finally Section V covers the conclusion and further work.

II. Inverter Model And MPC Control

The Continuous Control Set Model Predictive Control (CCS-MPC) methodology requires a model to be created that represents the inverter and its reactive coupling with the grid. Line currents in an AC/DC converter with RL filter are modelled in Section A, with the control methodology and volt-var control covered in Section B.

A. Modelling of RL filter Line Currents in dq Synchronous Frame

To create a predictive algorithm for control, the inverter line currents are modelled over an RL filter in a *dq* synchronous reference frame. In matrix form, the output voltage of the converter is represented in (1).

$$\begin{bmatrix} V_a \\ V_b \\ V_c \end{bmatrix} = \begin{bmatrix} R_f & 0 & 0 \\ 0 & R_f & 0 \\ 0 & 0 & R_f \end{bmatrix} \begin{bmatrix} i_a \\ i_b \\ i_c \end{bmatrix} + \begin{bmatrix} L_f & 0 & 0 \\ 0 & L_f & 0 \\ 0 & 0 & L_f \end{bmatrix} \frac{a}{a} \begin{bmatrix} i_a \\ i_b \\ i_c \end{bmatrix} + \begin{bmatrix} V_a \\ V_b \\ V_c \end{bmatrix} \quad (1)$$

Simplifying (1):

$$V_{D\ t} = \left(R_f * i_g\right) + L_f \frac{a i_g}{a} + V_g \quad (2)$$

$$V_a \quad = \frac{2}{3}[V_a \ + aV_b \ + a^2 V_c \ ] \quad (3)$$

$$i_g = \frac{2}{3}[i_a \ + a i_b \ + a^2 i_c \ ] \quad (4)$$

$$V_g = \frac{2}{3}[V_a \ + aV_b \ + a^2 V_c \ ] \quad (5)$$

$$a = e^{j\frac{2\pi}{3}} \quad (6)$$

Re-arranging (2) for $\frac{a i_g}{a}$:

$$\frac{a i_g}{a} = -\frac{R_f}{L_f} i_g + \frac{1}{L_f} V_D \quad - \frac{1}{L_f} V_g \quad (7)$$

Represented in matrix form in continuous time:

$$\frac{a}{a}\begin{bmatrix} i_a \\ i_b \\ i_c \end{bmatrix} = \underbrace{\begin{bmatrix} -R_f/L_f & 0 & 0 \\ 0 & -R_f/L_f & 0 \\ 0 & 0 & -R_f/L_f \end{bmatrix}}_{\dot{A}} \begin{bmatrix} i_a\ (t) \\ i_b\ (t) \\ i_c\ (t) \end{bmatrix} +$$

$$\underbrace{\begin{bmatrix} 1/L_f & 0 & 0 \\ 0 & 1/L_f & 0 \\ 0 & 0 & 1/L_f \end{bmatrix}}_{\dot{B}} \begin{bmatrix} V_a\ (t) \\ V_b\ (t) \\ V_c\ (t) \end{bmatrix} + \underbrace{\begin{bmatrix} -1/L_f & 0 & 0 \\ 0 & -1/L_f & 0 \\ 0 & 0 & -1/L_f \end{bmatrix}}_{\dot{B}} \begin{bmatrix} V_a\ (t) \\ V_b\ (t) \\ V_c\ (t) \end{bmatrix} \quad (8)$$

Simplifying (8):

$$\frac{a i_g}{a} = A i_g + B_i V_n + B_g V_g \quad (9)$$

Before translating into continuous time, the *abc* matrix in (1) is transformed into the synchronous *DQ* frame through a Clarke transform represented by (10) to give (11).

$$\begin{bmatrix} V_a \\ V_q \end{bmatrix} = \left(\frac{2}{3}\right) \begin{bmatrix} C & \cos(\theta - \frac{2\pi}{3}) & \cos(\theta - \frac{4\pi}{3}) \\ -S & -S\ (\theta - \frac{2\pi}{3}) & -S\ (\theta - \frac{4\pi}{3}) \end{bmatrix} \begin{bmatrix} V_a \\ V_b \\ V_c \end{bmatrix} \quad (10)$$

$$\begin{bmatrix} V_a \\ V_q \end{bmatrix} = \begin{bmatrix} R_f & -\omega_g L_f \\ \omega_g L_f & R_f \end{bmatrix} \begin{bmatrix} i_a \\ i_q \end{bmatrix} + \begin{bmatrix} L_f & 0 \\ 0 & L_f \end{bmatrix} \frac{a}{a} \begin{bmatrix} i_a \\ i_q \end{bmatrix} + \begin{bmatrix} V_a \\ V_q \end{bmatrix} \quad (11)$$

B. Inverter Control

In a 2-level, 6 switch voltage source inverter (2L-VSI) there are 8 possible switching states as represented in Table 1, along with output voltages of each phase. Under the proposed CCS-MPC control methodology, the goal of the inverter control is to output a preferred V_d and V_q quantity into a pulse width modulator via an *abc* transformation.

TABLE I
Switching Table for 2L Inverter

State	Activated Switch	V_a	V_b	V_c
1	1,3,5	0	0	0
2	1,4,6	$\left(\frac{2}{3}\right)V_L$	$-\left(\frac{1}{3}\right)V_L$	$-\left(\frac{1}{3}\right)V_D$
3	1,3,6	$\left(\frac{1}{3}\right)V_L$	$\left(\frac{1}{3}\right)V_D$	$-\left(\frac{2}{3}\right)V_D$
4	2,3,6	$-\left(\frac{1}{3}\right)V_L$	$\left(\frac{2}{3}\right)V_D$	$-\left(\frac{1}{3}\right)V_D$
5	2,3,5	$-\left(\frac{2}{3}\right)V_L$	$\left(\frac{1}{3}\right)V_D$	$\left(\frac{1}{3}\right)V_D$
6	2,4,5	$-\left(\frac{1}{3}\right)V_L$	$-\left(\frac{1}{3}\right)V_L$	$\left(\frac{2}{3}\right)V_D$
7	1,4,5	$\left(\frac{1}{3}\right)V_L$	$-\left(\frac{2}{3}\right)V_L$	$\left(\frac{1}{3}\right)V_D$
8	2,4,6	0	0	0

To convert output voltages from the switching table in Table 1, a synchronous rotating frame output must be provided. Converting this output voltage from *abc* into *DQ* uses a Park transform to convert from *abc* into α stationary frame, using (12), before conversion from α to *DQ* synchronous frame in (13).

$$T_{a\ \to a} = \left(\frac{2}{3}\right)\begin{bmatrix} 1 & -0.5 & -0.5 \\ 0 & \frac{\sqrt{3}}{2} & -\frac{\sqrt{3}}{2} \end{bmatrix} \quad (12)$$

$$T_{\alpha\ \to D} = \begin{bmatrix} C & S \\ -S & C \end{bmatrix} \quad (13)$$

$$V_{n,a} = V_D * T_{\alpha\ \to D} * T_{a\ \to \alpha} * \begin{bmatrix} S_a \\ S_b \\ S_c \end{bmatrix} \quad (14)$$

This converted output voltage from (14) is used to calculate line currents. Simplifying (11):

$$V_{n,a} = \left(R_f + j\omega_g L_f\right) i_{g,a} + L_f \left(\frac{a i_{g,a}}{a}\right) + V_{g,a} \quad (15)$$

Re-arranging (15) for line currents in continuous time.

$$\underbrace{\frac{a}{a}\begin{bmatrix} i_a\ (t) \\ i_q\ (t) \end{bmatrix}}_{\dot{x}(t)} = \underbrace{\begin{bmatrix} -R_f/L_f & \omega_g \\ -\omega_g & -R_f/L_f \end{bmatrix}}_{\dot{A}} \underbrace{\begin{bmatrix} i_a\ (t) \\ i_q\ (t) \end{bmatrix}}_{x(t)} +$$

$$\underbrace{\begin{bmatrix} 1/L_f & 0 \\ 0 & 1/L_f \end{bmatrix}}_{\dot{B}_n} \underbrace{\begin{bmatrix} V_a\ (t) \\ V_q\ (t) \end{bmatrix}}_{V_n(t)} + \underbrace{\begin{bmatrix} -1/L_f & 0 \\ 0 & -1/L_f \end{bmatrix}}_{\dot{B}_g} \underbrace{\begin{bmatrix} V_a\ (t) \\ V_q\ (t) \end{bmatrix}}_{V_g(t)} \quad (16)$$

Using forward Euler approximation (17) with T_s as the sampling rate, a discrete time model can be produced.

$$x(k+1) \approx x(k) + \left\{\frac{d\ (t)}{d}\right\} T_s, t = k \tag{17}$$

$$\Phi \approx \begin{bmatrix} 1 - (\frac{R_f T_s}{L_f}) & \omega_g T_s \\ -\omega_g T_s & 1 - (\frac{R_f T_s}{L_f}) \end{bmatrix} \tag{18}$$

$$\Gamma_n \approx \begin{bmatrix} T_s/L_f & 0 \\ 0 & T_s/L_f \end{bmatrix} \tag{19}$$

$$\Gamma_g \approx \begin{bmatrix} -T_s/L_f & 0 \\ 0 & -T_s/L_f \end{bmatrix} \tag{20}$$

Combining (16) with (18), (19) and (20), a discrete time model for line currents is produced.

$$\begin{bmatrix} i_d\ (k+1) \\ i_q\ (k+1) \end{bmatrix} = \Phi \begin{bmatrix} i_d\ (k) \\ i_q\ (k) \end{bmatrix} + \Gamma_n \begin{bmatrix} V_d\ (t) \\ V_q\ (t) \end{bmatrix} + \Gamma_g \begin{bmatrix} V_d\ (t) \\ V_q\ (t) \end{bmatrix} \tag{21}$$

Using the output voltages in Table 1 with (14) the output current in (21), and the sensed grid voltage, the output power and reactive power can be predicted.

$$P_o\ (k+1) = \left(\frac{3}{2}\right)\left(i_d\ (k+1)V_d\ (k+1) + i_q\ (k+1)V_q\ (k+1)\right) \tag{22}$$

$$Q_o\ (k+1) = \left(\frac{3}{2}\right)\left(i_d\ (k+1)V_q\ (k+1) + i_q\ (k+1)V_d\ (k+1)\right) \tag{23}$$

Owing to the DC nature of synchronous rotating frame values of V_g, it can be assumed that $V_g(k+1) \approx V_g(k)$.

$$P_o\ (k+1) \approx \left(\frac{3}{2}\right)\left(i_d\ (k+1)V_d\ (k) + i_q\ (k+1)V_q\ (k)\right) \tag{24}$$

$$Q_o\ (k+1) \approx \left(\frac{3}{2}\right)\left(i_d\ (k+1)V_q\ (k) + i_q\ (k+1)V_d\ (k)\right) \tag{25}$$

The cost function forms part of the iterative comparison process which drives the MPC inverter. With the requirement to control both active power and reactive power, the MPC control will calculate these with (24) and (25), before comparing to a reference.

$$g_o\ = \lambda_p\left(P_r\ - P_o\ \right)^2 + \lambda_q\left(Q_r\ - Q_o\ \right)^2 \tag{26}$$

Where, λ_p and λ_q are relative weighting factors and are set to one using per-unit weighting theory [18]. The goal of the algorithm is to predict and control an output power and reactive power that will trend g_o towards 0 with the provided reference active and reactive powers. Fig. 2 details the iterative process the MPC algorithm uses to calculate the ideal switching state for the inverter.

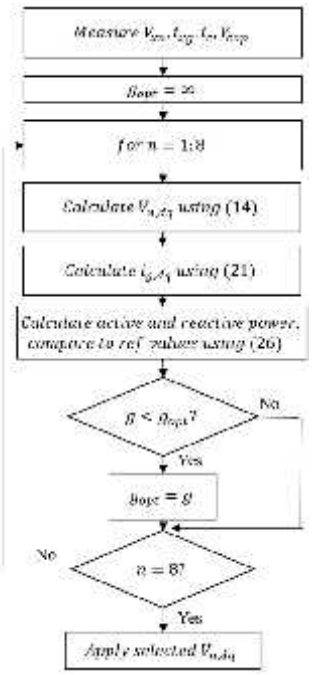

Fig. 2. Iterative predictive algorithm flow chart

The output of the MPC algorithm takes the form of V_d and V_q, which is converted into an *abc* signal, before being translated into a PWM output. This allows for a switching state to be set at a known frequency, which aids in designing the output filter.

A requirement of grid-supporting inverters is reactive power control. The output power factor of the inverter can be manipulated in low or high-voltage events in the grid; by setting a defined low and high voltage limit, the inverter can use the algorithm in Fig. 4 to determine the reference power factor. Using this generated power factor allows a reference reactive power, Q_r , to be set automatically.

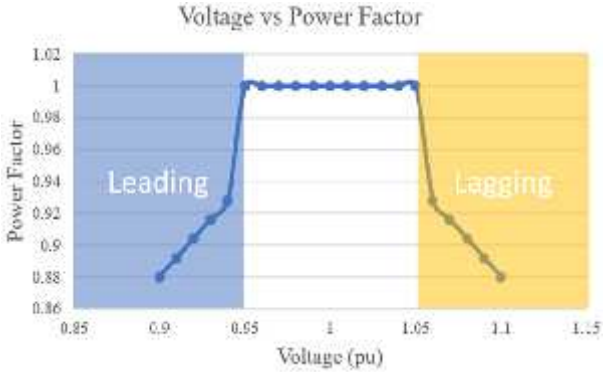

Fig. 3. Voltage vs power factor for λ_V $_{-V}$ = 1.2

Using a scaling factor λ_V $_{-V}$, the resultant power factor is a function of the difference between V_p $_{,Lc}$ $_{/Nom}$ and V_p $_{,g}$.

$$p\ = 1 - (\lambda_V\ _{-V}\ * \left(V_p\ _{,Lc}\ - V_p\ _{,g}\ \right)) \tag{27}$$

$$p\ = 1 - (\lambda_V\ _{-V}\ * \left(V_p\ _{,g}\ - V_p\ _{,Nom}\right)) \tag{28}$$

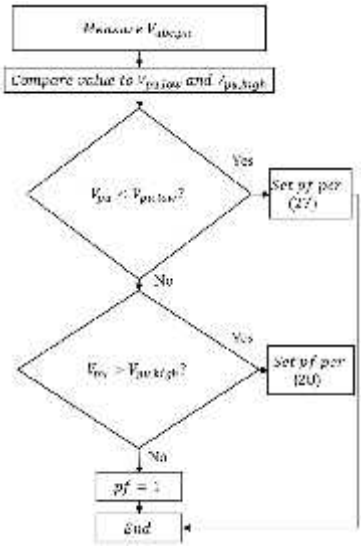

Fig. 4. Iterative Volt-Var process

C. LC Filter Design

Suppression of output switching harmonics is completed by use of an LC filter. The base impedance of the inverter is determined using (27) with the nominal power P_{in} and output line to line voltage V_{L-L}, and selecting a cutoff frequency f_c allows the filter components L_f and C_f to be determined.

$$Z_b = \frac{V_{L-L}^2}{P_{in}} \quad (27)$$

$$L_f = \frac{Z_b}{\pi * f_c} \quad (28)$$

$$C_f = \frac{1}{Z_b * \pi * f_c} \quad (29)$$

III. Simulation of MPC Based Solar PV System

A. Overview

To verify the algorithm, a grid-connected 2 level 3-phase PV system shown in Fig. 5 was designed and implemented in MATLAB/SimPowerSystem . Table 2 details the system parameters of the model.

TABLE 2
SIMULATION SYSTEM PARAMETERS

Parameter	Value
DC Voltage	609V
DC Link Capacitor	330uF
Rated Power	13.43kW
Rated Reactive Power	5.97kVAR
Output Voltage	240VRMS
Filter Inductor	8mH
Filter Capacitor	50uF
Anti-ringing resistance	25Ω
PWM Switching Frequency	20kHz
Load 1	41.7kVA
Load 2	66kVA
Grid Frequency	50Hz

The PV array is controlled by Perturb & Observe MPPT and provides the reference current i_{ref} to the model predictive controller. Sample time *Ts* is set to 10μ .

The utility grid is modelled as a 120kV voltage source, stepped down to 25kV with a local 30MVA load, feeding the inverter and Load 1 & 2 (41.7 and 66kVA respectively) through a short feeder. The voltage is stepped down to 240V through a 60kVA transformer. To test Volt-Var control, Q_{ref} was set to 0 initially, before the Volt-Var control is activated for a second run. The scaling factor λ_{V_V} was be tested at 5 different levels to analyse its effect on grid voltage V_{pu} under load, and compared to no Volt-Var control.

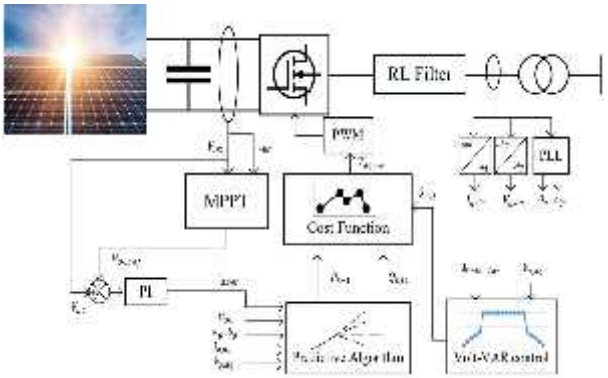

Fig. 5. High-level simulation control overview

B. Results and Discussion

The simulation scenario lasts for 1 second with Load 1, with an additional load (Load 2) being actuated through a breaker at T= 0.5s and disconnected at T=0.9s. This second load is designed to cause a voltage drop in the local area from $V_{pu} = 0.96 \rightarrow 0.945$ to trigger an increase in reactive power output from the inverter to compensate.

Fig. 6 shows the grid, inverter, and load active powers during the testing. Fig. 7, 8 & 9 show the output voltage and current waveforms during the load change at T=0.5s, with the voltage waveform reducing in magnitude due to increased current draw through the transformer and transmission lines. The output current in Fig. 7 increases in magnitude due to the Volt-Var control forcing a change to a leading power factor for the inverter.

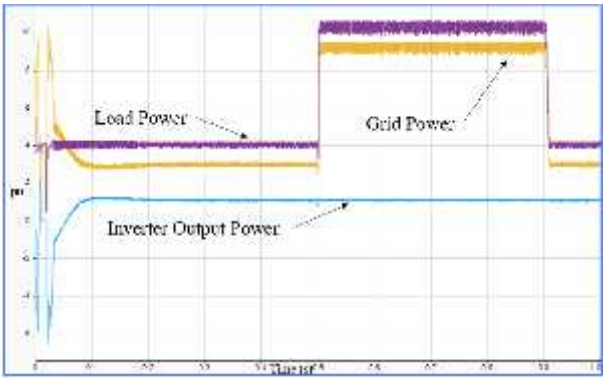

Fig. 6. Inverter, load, and grid powers (pu)

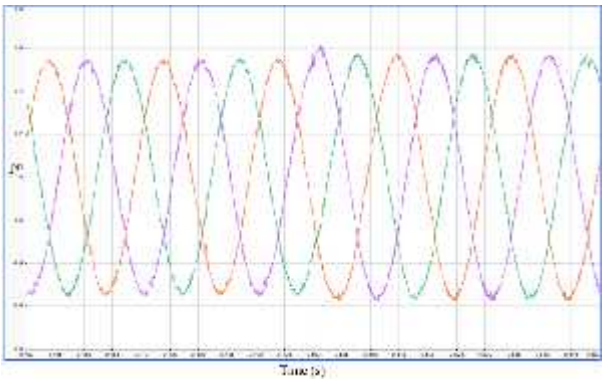

Fig. 7. Inverter output current across T=0.5s (pu)

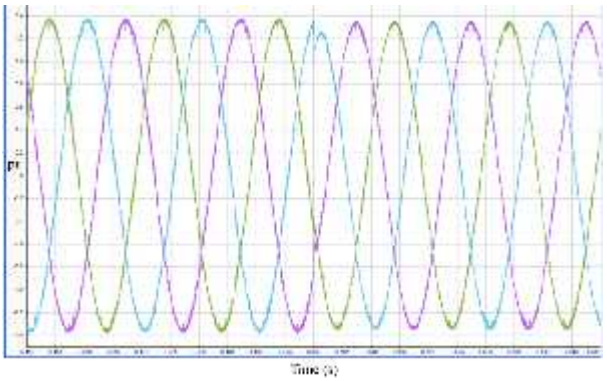

Fig. 8. Inverter output voltage across T=0.5s (pu)

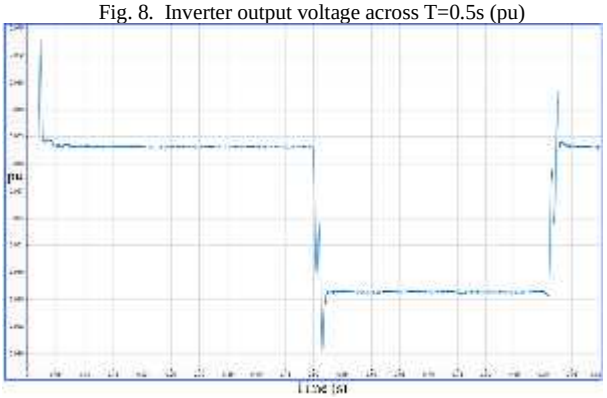

Fig. 9. Voltage RMS (pu)

The grid, load, and inverter reactive powers are presented in Fig. 10 & 11, showing an increase in absorption of reactive power at t=0.5s. The inverter injects an additional 0.2pu of reactive power when the measured voltage decreases below the set point at $V_{pi} = 0.96$.

Fig. 12 shows the V_{pi} changes as the additional load is introduced, showing the difference between unity power output and Volt-Var control.

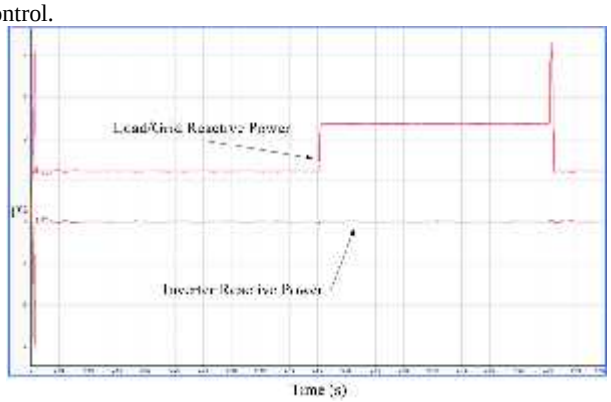

Fig. 10. Grid, load, and inverter reactive power with no Volt-Var control (pu)

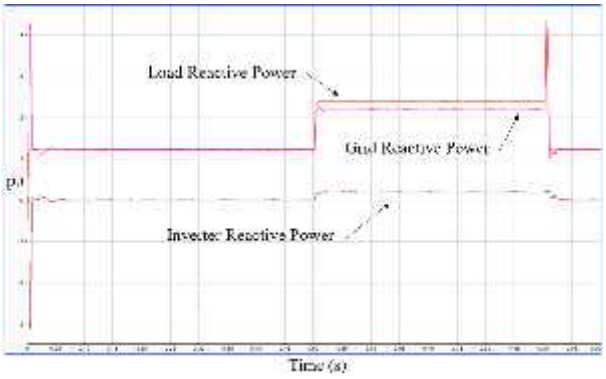

Fig. 11. Grid, load, and inverter reactive power with Volt-Var control (pu)

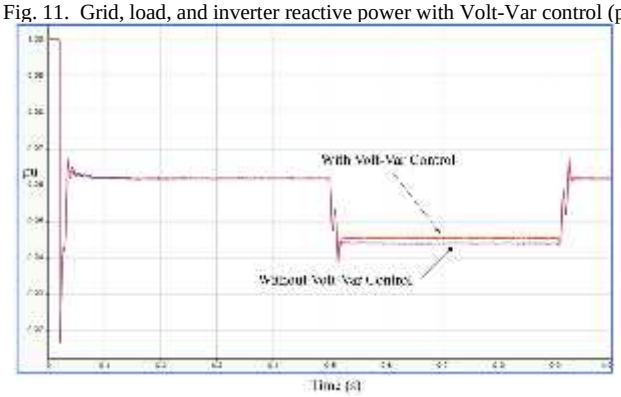

Fig. 12. Grid voltage with and without Volt-Var control (pu)

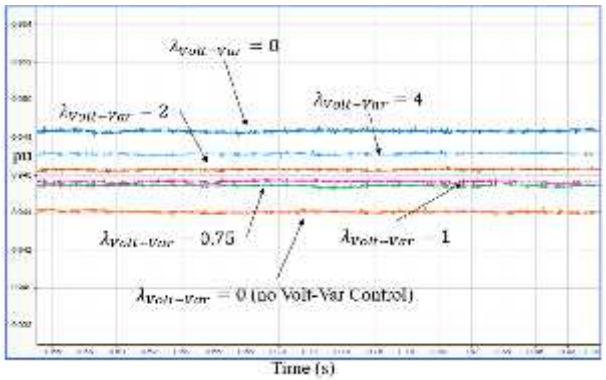

Fig. 13. Grid voltage under load with varying $\lambda_{V \_ V}$ scaling factors (pu)

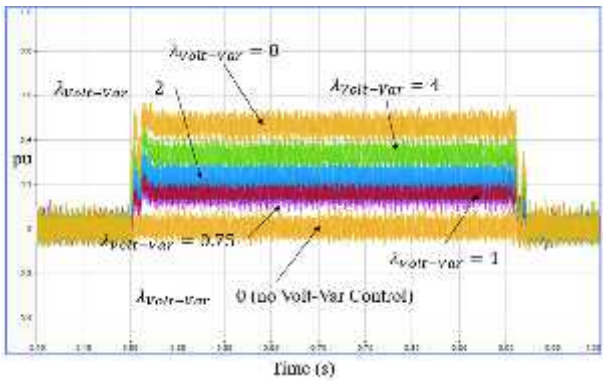

Fig. 14. Reactive power output of inverter under different $\lambda_{V \_ V}$ scaling factors (pu)

Comparing different scaling factors in Fig. 13 shows an increase in grid voltage while under load, allowing for better local voltage regulation.

Fig. 15 & 16 show the FFT analysis of the output waveforms of the inverter. The voltage analysis shows some increase in signals for the 142nd, 151st and 154th harmonics, however overall THD is within acceptable levels, with low harmonics present in high frequencies above 20kHz.

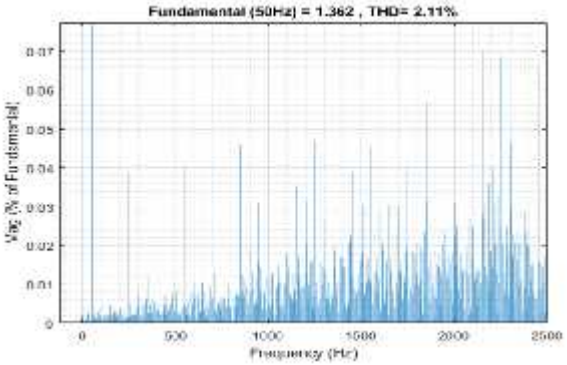

Fig. 15. FFT analysis of voltage waveform

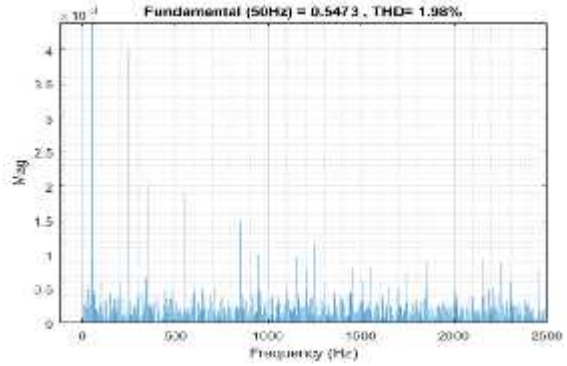

Fig. 16. FFT analysis of current waveform

IV. Conclusion

This e-paper presents a continuous control set model predictive control for a grid-tied inverter under simulated demands. The results show good response to changing load demands through the injection or absorption of reactive power, with the scale of variance able to be changed through a scaling factor. Increases in load show little perturbation of the output signals from the inverter. The output signal has little distortion through an LC filter especially in higher frequencies. Meeting the requirements for *IEEE 1547.2018* to ensure grid stability into the future is an important challenge to meet, and the proposed model predictive control for an inverter using an adjustable power factor scaling factor can facilitate meeting the Volt-Var requirements for strengthening grid-supporting functions.

The CCS-MPC control method shown allows for a reduction in tuning difficulties with a single PI controller only, however PWM control is still required. Future work will be around Finite Control Set methodology with switching frequency weighting factors to remove pulse width modulation, allowing for a permissible switching frequency range to aid in filter design, incorporating Frequency-Watt and active power-reactive power scaling, as well as a hardware validation of the simulation, using a Solid-State Transformer (SST) for galvanic isolation and DC-bus voltage regulation in a 3L inverter topology

V. References

[1] D. Condon, D. McPhail and D. Ingram, "Application of low voltage STATCOM to correct voltage issues caused by Inverter Energy Systems," in *AUPEC 2016*, Brisbane, Australia, 2016.

[2] D. Zhang and J. Fletcher, "OPeration of Autonomous AC Microgrid at Constant Frequency and with Reactive Power Generation from Grid-forming, Grid-supporting and Grid-feeding generators," in *TENCON*, Jeju, Korea, 2018.

[3] Standards Australia, *Grid connection of energy systems via inverters Part 2: Inverter Requirements*, 2015.

[4] IEEE, *IEEE Standard for Interconnection and Interoperability of Distributed Energy Resources with Associated Energy Power Systems Interfaces*, New York, 2018.

[5] U. Markovic, O. Stanojev, P. Aristidou and G. Hug, "Partial Grid Forming Concept for 100% Inverter-Based Transmission Systems," in *IEEE Power &Energy Society General Meeting (PESGM)*, Portland, OR, 2018.

[6] R. H. Lasseter, Z. Chen and D. Pattabiraman, "Grid-Forming Inverters: A Critical Asset for the Power Grid," *IEEE Journal of Emerging and Selected Topics in Power Electronics*, vol. 8, no. 2, pp. 925-936, 2020.

[7] K. H. Ang and G. L. Y. Ching, "PID control system analysis, design, and technology," *IEEE Transactions on Control Systems Technology*, vol. 13, no. 4, pp. 559-577, 2014.

[8] Y. Shan, J. Hu, M. Liu and J. G. J. Zhu, "Model Predictive Voltage and Power Control of Islanded PV-Battery Microgrids With Washout-Filter-Based Power Sharing Strategy," *IEEE Transactions on Power Electronics* , vol. 35, no. 2, pp. 1224-1238, 2020.

[9] Q. Ye, R. Mo and H. Li, "Multiple Resonances Mitigation of Paralleled Inverters in a Solid-State Transformer (SST) Enabled AC Microgrid," *IEEE Transactions on Smart Grid*, vol. 9, no. 5, pp. 4744-4755, 2018.

[10] K. Oue, S. Sano, T. Kato and K. Inoue, "Stability Analysis of Grid-Forming Inverter in DQ Frequency Domain," in *20th Workshop on Control and Modeling for Power Electronics (COMPEL)*, Toronto, ON, 2019.

[11] C. S. Lim and S. S. Lee, "Comparison of Current Control Strategies Based on FCS-MPC and D-PI-PWM Control for Actively Damped VSCs With LCL-Filters," *IEEE Access*, vol. 7, pp. 112410-112423, 2019.

[12] S. Bayhan and M. A.-R. H. Trabelsi, "Model Predictivie Control of Z-Source Four-Leg Inverter for Standalone Photovoltaic System with Unbalanced Load," in *IEEE Applied Power Electronics Conference and Exposition (APEC)*, Long Beach, CA, 2016.

[13] Y. L. Y. Liu, B. Ge and H. Abu-Rub, "Interactive Grid Interfacint System by Matrix-Converter-Based Solid State-Transformer with Model Predictive Control," *IEEE Transactions on Industrial Informatics*, vol. 16, no. 4, pp. 2533-2542, 2020.

[14] Y. Shan, J. Hu and J. M. Guerrero, "A Model Predictive Control Method for PV and Energy Storage Systems with Voltage Support Capability," *IEEE Transactions on Smart Grid*, vol. 11, no. 2, pp. 1018-1030, 2020.

[15] M. Novak, T. Dragicevic and F. Blaabjerg, "Weighting Factor Design based on Artificial Neural Network for Finite Set MPC operated 3L-NPC converter," in *IEEE Applied Power Electronics Conference and Exposition (APEC)*, Anaheim, CA, 2019.

[16] M. B. Shadmand, R. S. Balog and H. Abu-Rub, "Auto-tuning the cost function weight factors in a model predictive controller for a matrix converter VAR compensator," in *IEEE Energy Conversion Congress and Exposition (ECCE)*, Montreal, QC, 2015.

[17] R. E. Perez-Guzman and M. Rivera, "Weighting Factor Selection in Power Converters Based on Model Predictive Control," in *2020 Congreso Estudiantil de Electrónica y Electricidad (INGELECTRA)*, Santiago, Chile, 2020.

[18] V. Yaramasu and B. Wu, Model Predictive Control of Wind Energy Conversion Systems, Hoboken: John Wiley & Sons, 2017.

[19] E. Demirok, P. C. Gonzalez, K. H. B. Frederiksen, D. Sera and P. T. R. Rodriguez, "Local Reactive Power Control Methods for Overvoltage Prevention of Distributed Solar Inverters in Low-Voltage Grids," *Journal of Photovoltaics*, vol. 1, no. 2, pp. 174-183, 2011.

[20] G. Kerber, R. Witzmannm and H. Sapple, "Voltage limitation by autonomous reactive power control of grid connected photovoltaic inverters," in *Compatibility and Power Electronics*, Badajoz, 2009.

[21] R. K. Varma and R. Salehi, "SSR Mitigation With a New Control of PV Solar Farm as STATCOM (PV-STACOM)," *IEEE Transactions on Susttainable Energy*, vol. 8, no. 4, pp. 1473-1484, 2017.

[22] R. K. Varma, S. A. Rahman, V. Sharma and T. Vanderheide, "Novel Control of a PV Solar System as STATCOM (PV-STATCOM) for Preventing Instability of Induction Motor Load," in *25th IEEE Canadian Conference on Electrical and Computer Engineering (CCECE)*, Montreal, QC, 2012.